



Numerical Study on the Effects of Bulbous Bow Shape to Improve the Hydrodynamic Characteristics of KCS Hull using CFD

Sajib Das^{1,*}, Md Mehrab Khan¹, Md. Mashud Karim¹

ARTICLE INFO

Article history:

Received 01 Aug 2024;
in revised from 08 Aug 2024;
accepted 14 Aug 2024.

Keywords:

STAR-CCM+, FVM, CAESES,
Bulbous Bow, Free Form Deformation.

ABSTRACT

One of the most important aspects of designing a new ship to achieve improved hydrodynamic performance is improving the hull form. This study investigates the improvement of a hull form (KCS) through the utilization of the Free Form Deformation (FFD) method in CAESES and STAR-CCM+. The main purpose of this investigation is on improving the KCS hull by investigating various bulbous bow shapes. The Free Form Deformation (FFD) method was employed to modify the geometry of the bulbous bow, while the STAR-CCM+ software was applied for the simulation. The variables considered for improvement were the length, width, angle, height, and combination these factors. As a consequence of the investigation into seven distinct cases, case number seven exhibited the most favorable outcomes exhibiting the minimum resistance and having the lowest total resistance coefficient the least in lowest Froude number. This will enhance fuel efficiency and help the environment and economic system. In addition to having an impact on the ship's resistance, the improved bulbous bow shape of the hull also will have an impact on the hydrodynamic performance.

© SEECMAR | All rights reserved

1. Introduction.

The improvement of hydrodynamic performance in marine vehicles has garnered significant interest among researchers because of its potential to minimize resistance and improve structural design [Nazemian and Ghadimi, 2020]. As, Optimizing the hydrodynamic characteristics of the hull form is of utmost importance when it comes to the preliminary design stage of ships. Studies on optimizing hull shape through computer modeling have been used increasingly to make ships that use less energy, and are better for the environment, and are economically profited due to computer-aided design (CAD) technological improvement [Zhang and Kim, 2020]. Computational Fluid Dynamics (CFD) has emerged as a highly influential technique for industry and research in recent years, offering a convenient, reliable and cost-effective means of predicting a ship's hydrody-

dynamic performance allowing for the visualization of flow patterns and critical aspects that are crucial for designing a new ship. But Experimental Fluid Dynamics (EFD) remains the most precise approach for predicting ship performance, it requires high cost and facilities which has limited its use [Yu, et al., 2019].

The approach to optimization as a whole relies heavily on the hull form modification. Currently, the bulbous bow is increasingly being incorporated into various types of marine vessels. The combination of the bulbous bow wave and the ship front wave can provide beneficial interference, resulting in a significant reduction in wave resistance as well as total resistance [Li, et al., 2016]. An improved bulbous bow shape can further reduce the total resistance.

There are several methods available to alter the bulbous bow in order to achieve the most optimum shape.

Recently, parametric modeling and the Free-Form Deformation (FFD) are the most predominant methods that have been employed consistently to alter the geometry of a bulbous bow for attaining an improve shape in order to reduce resistance. Parametric modeling is a process of controlling and altering the

¹Department of Naval Architecture and Marine Engineering, Bangladesh University of Engineering and Technology, Dhaka-1000, Bangladesh.

*Corresponding author: Sajib Das. E-mail Address: sajib-das005@gmail.com.

shape of the geometry using computational techniques which involve three distinct stages in computer-aided design (CAD) those are wireframe, surface, and solid modeling and it occurs algorithmically by utilizing parameters that represent geometric aspects of a design model [Feng, et al., 2021].

The process Free Form deformation (FFD) is a flexible geometric technique, initially introduced by Sederberg and Parry in 1986, that permits the modification of rigid bodies [Sederberg and Parry, 1986]. It can boost design flexibility, and simplify improvement of algorithm integration. In addition to its widespread application in a variety of fields, it has garnered a considerable amount of attention in hull geometry improvement [Liu, et al., 2021].

In this study, the main goal is to improve the KRISO Container Ship (KCS) hull for lowering total resistance in calm water. The simulations are carried out with the assistance of a commercial code called STAR-CCM+, which is discretized by the Finite Volume Method (FVM). The Free-Form Deformation (FFD) method, in conjunction with CAESES, was used to improve the bulbous bow's length, breadth, angle and combination of these. The bow section was improved by simulating seven possible hull configurations and comparing them. Finally, the hull with least resistance having improved bow shape is simulated at various Froude numbers.

2. Numerical Approach.

2.1. Background.

The foundation of Computational Fluid Dynamics rests upon three fundamental equations. Those are the Continuity equation, the Navier-Stokes equation, and the Energy equation. In this investigation, the Reynolds-averaged Navier-Stokes (RANS) equation was solved by the computational fluid dynamics (CFD) algorithm to simulate the behavior of unsteady turbulent flows around ship models. The computational domain is discretized using the Finite Volume Method (FVM) [Islam, et al., 2022]. STAR-CCM+ provides a diverse range of turbulence modeling choices such as $k - \epsilon$, $k - \omega$, and Reynolds Stress Transport. In this study, the $k - \epsilon$ turbulence model was used. Volume of Fluid (VOF) approach was employed for accurately capturing the free surface. The SIMPLE scheme is utilized for the purpose of solving the discretized momentum equations.

2.2. Governing Equation.

An appropriate assumption for the majority of fluid flows is that the flow is here incompressible, which simplifies the continuity equation and the momentum equation and avoids solving the energy equation. For an incompressible flow, the continuity equation and momentum equation are written as follows [Voxakis, 2012]:

Continuity equation:

$$\nabla \cdot \mathbf{U} = 0$$

Momentum equations:

$$\rho \frac{\partial \mathbf{U}}{\partial t} = -\nabla p + \mu \nabla^2 (\mathbf{U}) + \nabla \cdot \mathbf{T}_{Re} + \mathbf{S}_M$$

The variables in consideration are \mathbf{U} , ρ , μ , and p . \mathbf{U} is the averaged velocity vector, ρ stands for fluid density, μ represents dynamic viscosity, and p represents the averaged pressure field., \mathbf{T}_{Re} is the tensor of Reynolds stresses and \mathbf{S}_M is the momentum source vector.

2.3. Volume of Fluid (VOF) Method.

To monitor the interface between multiphase (air and water) VOF method is used. The general transpose equation for volume fraction is represented below:

$$\frac{\partial(\alpha\Phi)}{\partial t} + \nabla \cdot (\alpha\Phi\mathbf{U}) = \nabla \cdot (\Gamma\nabla\Phi)$$

This equation can be reduced to [Voxakis, 2012]:

$$\frac{\partial\alpha}{\partial t} + \nabla \cdot (\alpha\mathbf{U}) = 0$$

Here, α is the volume fraction (ranging from 0 to 1) of a single fluid within a cell, \mathbf{U} represents the velocity field, Γ is the diffusivity coefficient Φ is a scalar field.

Where,

$\alpha = 0$; air

$0 < \alpha < 1$; interface

$\alpha = 1$; water

2.4. Turbulence Model.

In order to calculate turbulent flows using the RANS equations, it is crucial to use turbulence models that can precisely forecast the Reynolds stresses and scalar transport components [Versteeg and Malalasekera, 2006]. These models help in closing the system of mean flow equations. A turbulence model needs to be highly accurate, simple, cost-effective, and widely applicable in order to be used in a variety of CFD codes. From the existing various turbulence models, the $k - \epsilon$ turbulence model is used here. The $k - \epsilon$ turbulence model is a type of eddy viscosity model that consists of two equations. The $k - \epsilon$ turbulence model involves solving additional transport equations for the turbulent kinetic energy (k) and its dissipation rate (ϵ) to calculate the turbulent viscosity [Voxakis, 2012]:

The standard $k - \epsilon$ model uses the following transport equations for k and ϵ [Versteeg and Malalasekera, 2006].

$$\frac{\partial(\rho k)}{\partial t} + \text{div}(\rho k \mathbf{U}) = \text{div} \left[\frac{\mu_t}{\sigma_k} \text{grad} k \right] + 2\mu_t S_{ij} \cdot S_{ij} - \rho \epsilon$$

$$\frac{\partial(\rho \epsilon)}{\partial t} + \text{div}(\rho \epsilon \mathbf{U}) = \text{div} \left[\frac{\mu_t}{\sigma_\epsilon} \text{grad} \epsilon \right] + C_{1\epsilon} \frac{\epsilon}{k} 2\mu_t S_{ij} \cdot S_{ij} - C_{2\epsilon} \rho \frac{\epsilon^2}{k}$$

Where μ_t is the eddy viscosity, σ_ϵ and σ_k are Prandtl numbers, $C_{1\epsilon}$ and $C_{2\epsilon}$ are constant that correct proportionality between k and ϵ equations, S_{ij} is the rate of deformation.

3. Geometry and Test Condition.

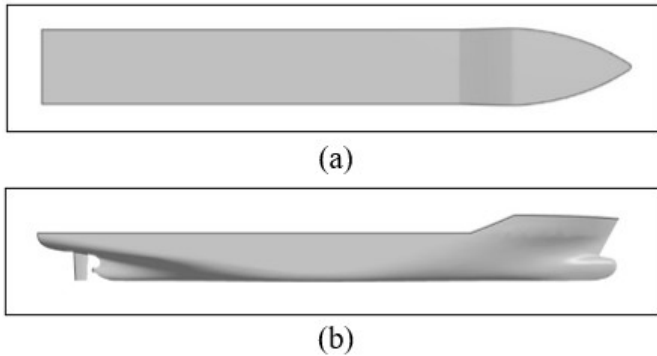
3.1. Geometry.

The model used in this investigation is a 7-meter-long KCS model featuring a bulbous bow. The geometry is shown in Figure 1, with specific attention given to the rudder. The KCS

model was specifically developed as a standardized model to create experimental data to verify CFD simulations [Hino, et al., 2020]. Additionally, it served as a benchmark model in the Tokyo 2015 CFD workshop on hydrodynamics.

The geometric parameters of the KCS model are shown in the following, and the scale ratio used in the current investigation is 31.599.

Figure 1: Geometry of KCS Hull. (a) Top view, (b) Side view.



Source: Authors.

Table 1: Principal particulars of KCS Hull.

Main Particulars		Full Scale	Model Scale
Length Between Perpendiculars	L_{PP} (m)	230	7.2786
Beam of Waterline	B_{WL} (m)	32.2	1.019
Depth	D (m)	19	0.6013
Draft	T_M (m)	10.8	0.3418
Displacement	∇ (m ³)	52030	1.649
Wetted Surface Area with rudder	S_0 (m ²)	9539	9.553
Moment of Inertia	K_{xx}/B	0.4	0.4
Moment of Inertia	K_{yy}/L_{PP}	0.25	0.25
Moment of Inertia	K_{zz}/L_{PP}	0.25	0.25

Source: Authors.

3.2. Test Condition.

To conduct the resistance test, calm water condition was used with a rudder attached to the hull. Initially, the current study does a numerical simulation based on the real model hull speed of 2.196 m/s ($Fr=0.26$). The gravity acceleration is 9.81 m/s². There exist experimental data in the Tokyo 2015 CFD workshop. The model test was conducted in calm water. After improving, the improve hull was tested at various speeds of different Froude numbers.

4. Bulbous Bow Modification.

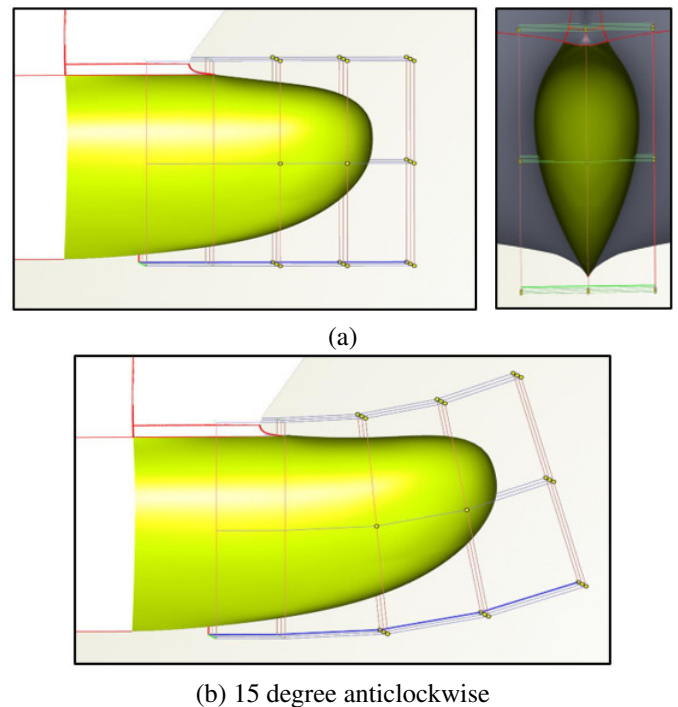
The basic concepts of FFD technology involve the followings, first determining the lattice, which is a cuboid based on the deformed region, and then linearly embedding the object to be deformed into the lattice through local coordinate transformation; next, defining a control point grid on the lattice to transform it into a three-dimensional body; and lastly, manipulating the control points to achieve the desired deformation [Hao, 2019].

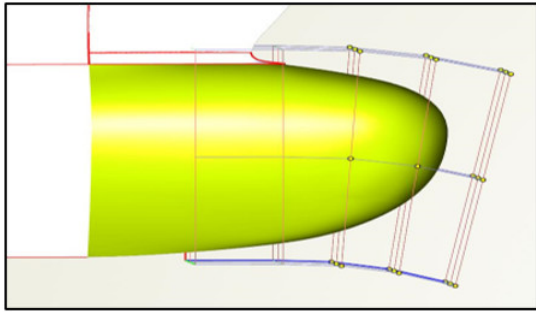
Prior to the introduction of FFD, all deformations had to be executed directly on an object. However, the FFD technique involves embedding an object in a space that is subsequently deformed [Sederberg and Parry, 1986]. An often used analogy for FFD is to envision an object enclosed within a parallelepiped made of transparent and pliable plastic. Deforming the lattice structure will cause a corresponding deformation of the thing contained within.

Bulb sizes significantly impact the bow wave and how the hull and bulb generate waves together. The ideal model was designed by varying bulb sizes (length, width, angle, height, and combination of these) to discover the shape that minimized ship total resistance. CAESES software is used to change the shape of the bulbous bow using the Free-Form Deformation (FFD) method. Seven different cases with different bulbous bow orientations were simulated in this study.

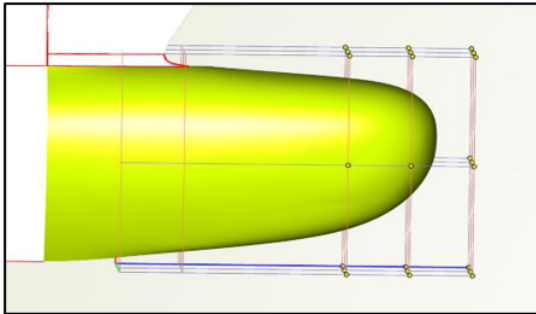
In order to acquire Case 7, it required several iterations and investigation by analyzing the outcomes from numerous computational fluid dynamics (CFD) simulations.

Figure 2: Parent bow (a) and Modified bows. (b) Case 1, (c) Case 2, (d) Case 3, (e) Case 4, (f) Case 5, (g) Case 6, (h) Case 7.

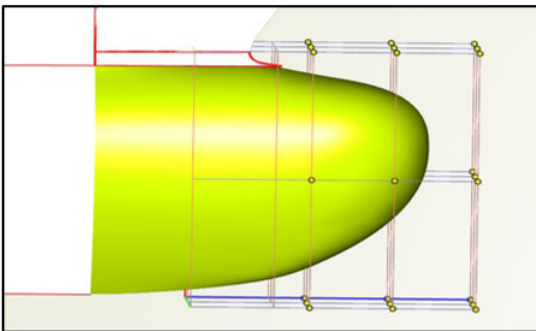




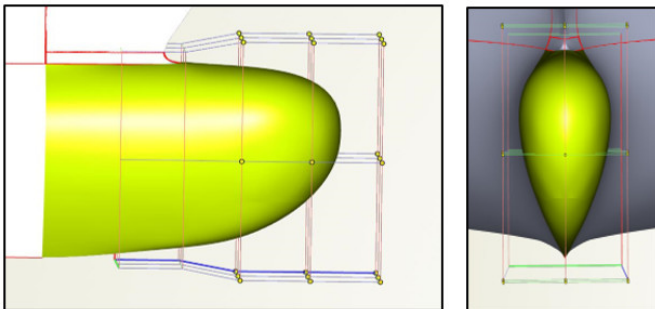
(c) 10 degree clockwise



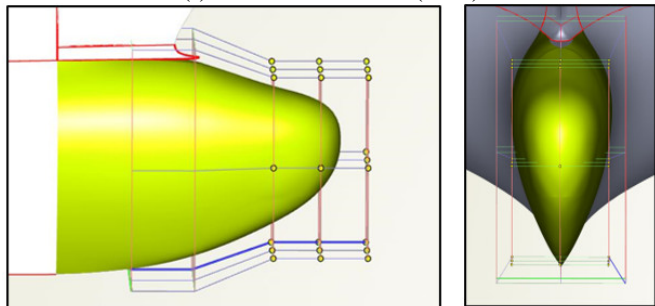
(d) Increased length 14% (0.019 LPP)



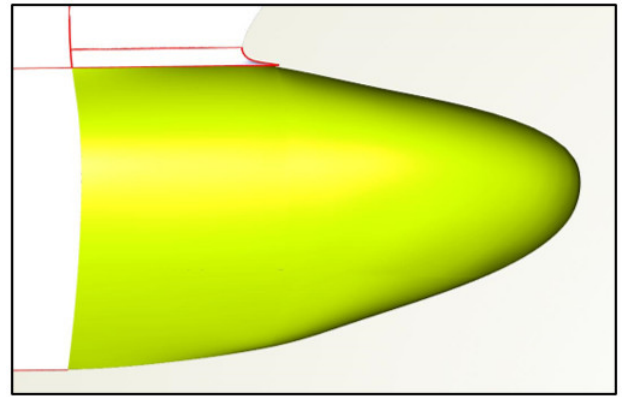
(e) Decrease length 5% (0.007 LPP)



(f) Increased Breadth (10%)



(f) Decrease Breadth (25%)



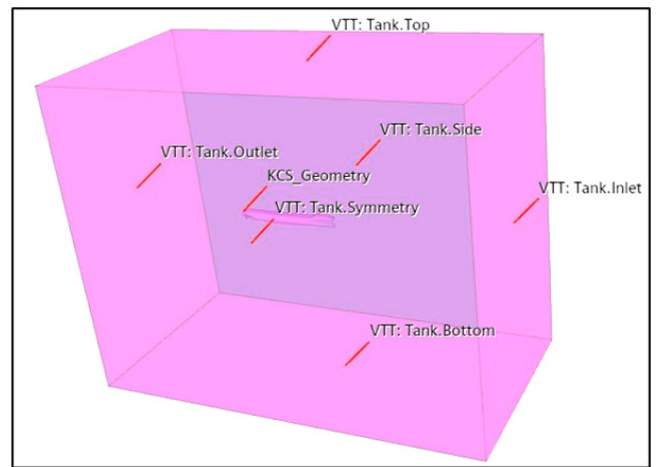
(h) Length 0.027 LPP, Height 2% increased, 15 degree clockwise rotation

Source: Authors.

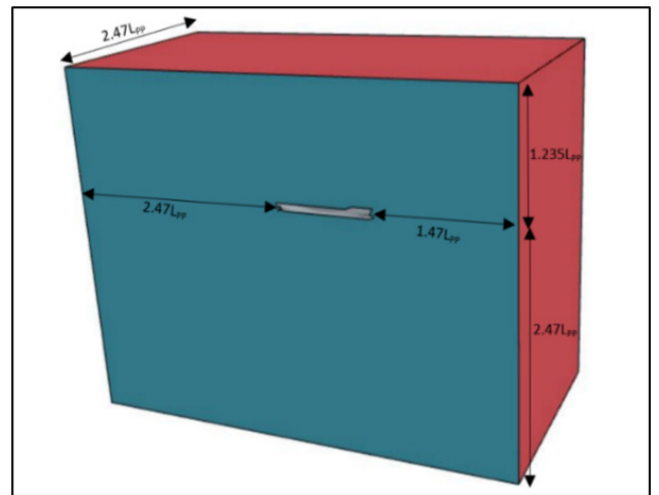
5. Computational Domain.

The KCS model hull is positioned inside a computational domain, as illustrated in Figure 3.

Figure 3: (a) Computational Domain, (b) Boundary Distances.



(a)



(b)

Source: Authors.

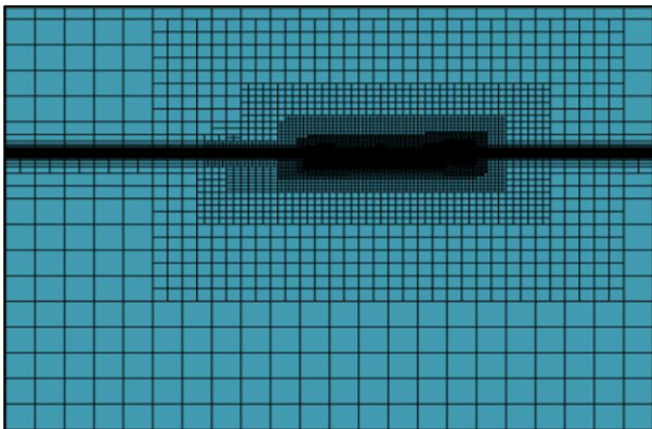
In this study, the origin of the region was set at aft perpendicular and still water level. The range of the domain extends in 3 directions, which are $-2.47L_{pp} < x < 2.47L_{pp}$, $0 < y < 2.47L_{pp}$, and $-1.235L_{pp} < z < 2.47L_{pp}$. Due to the symmetry, the simulation was conducted for half of the model. In all conditions. The boundary ranges from the ship model locations are illustrated below.

6. Mesh Generation.

For mesh operation, the unstructured trimmer mesh was used. To capture the free surface and complex and sharp edges, volumetric refinement was done to generate the volume mesh [Nazemian and Ghadimi, 2020]. Grid cells discretize partial differential equations and approximation algebraic equations using the finite volume method. Every mesh specification was given as a percentage of the base size. Except for the deck and stern, prism layers were made around the walls to more accurately resolve boundary layers close to solid surfaces. The All- $y+$ wall treatment combines elements of both the high-wall treatment and the low- $y+$ wall treatment, with the goal of simulating their effects on coarse and fine meshes, respectively [Franck, et al., 2017]. The Two-Layer Similar to the All $y+$ Wall Treatment, the All $y+$ Wall Treatment with a wall boundary requirement for ϵ that aligns with the two-layer formulation is known as All $y+$ Wall Treatment.

A total of six prism layers were used with a stretching factor of 1.5, and the thickness of the prism layer was an absolute size of 0.02m. The volume growth rate was selected slowly. Grids were created using base sizes 0.13 m, 0.1175 m and 0.1 m for grid independency, and the number of cells varied for each case, i.e., for Case 7, the number of cells was 685468 at 0.1 m of base size. The volume anisotropic reinforcement along the z -direction was applied close to the free surface to maintain a higher mesh quality. The mesh reinforcement design surrounding the body effectively was done to capture the Kelvin waves.

Figure 4: Mesh generation within flow domain.



Source: Authors.

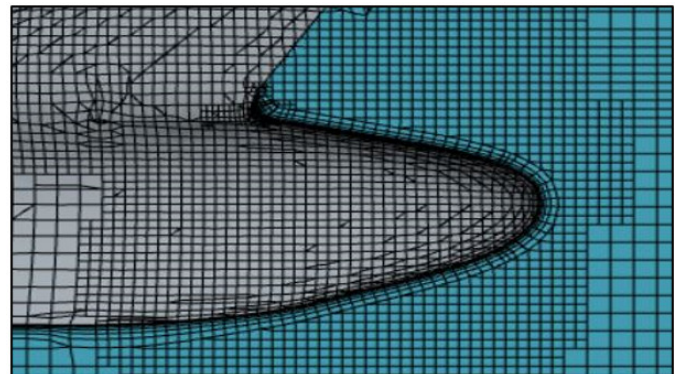
Enclosed is the magnified view following the creation of the

mesh, allowing for a more detailed investigation of the distribution of the mesh around the hull, bows, and wake zone.

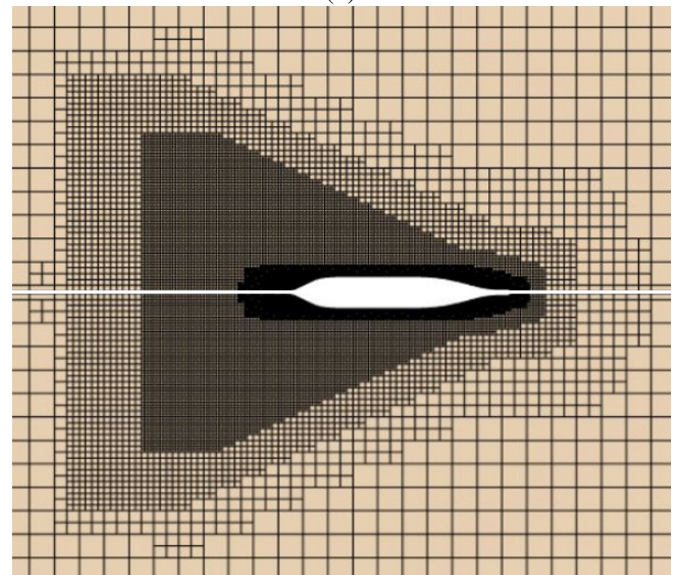
Figure 5: Mesh refinement (a) around the hull (b) around the bow (c) to capture the Kelvin wake pattern.



(a)



(b)



(c)

Source: Authors.

In the case of the KCS parent model, three separate grids are created when the Froude number is set to 0.26. These grids are used to calculate the total drag and total resistance coefficient in order to perform a grid independence test. Mesh number three exhibits the most favorable outcomes with the least amount of variation.

Table 2: Total Drag at different mesh at Froude Number 0.26.

Mesh Number	Base Mesh Size (m)	Cell Numbers	Drag (half body) (N)	Total Drag (N)
1	0.13	423458	41.47	82.94
2	0.1175	482210	41.65	83.3
3	0.1	671951	41.66	83.32

Source: Authors.

Table 3: Total Resistance Coefficient comparison of CFD and EFD results at Froude Number 0.26.

Mesh Number	Froude Number	$C_T \times 10^3$ (CFD)	$C_T \times 10^3$ (Exp. by Hino et al., 2015)	Deviation (%)
1	0.26	3.601	3.711	2.96
2		3.616		2.56
3		3.6173		2.525

Source: Authors.

7. Boundary Conditions.

The subsequent boundary conditions are imposed on the domain's faces:

Table 4: Boundary Conditions.

Boundary	Type
Tank.Bottom	Velocity Inlet
Tank.Outlet	Pressure Outlet
Tank.Side	Symmetry Plane
Tank.Inlet	Velocity Inlet
Tank.Symmetry	Symmetry Plane
Tank.Top	Velocity Inlet

Source: Authors.

The hull's boundaries are specified as a wall with no-slip conditions. Eulerian multiphase simulations, including two phases, namely air and water, are generated.

8. Result and Discussion.

The simulation has been carried out for all the cases as well as for the parent hull. In STAR-CCM+ to determine the total resistance (Pressure force and shear force) for all the cases, the Dynamic Fluid Body Interaction module was selected. According to ITTC guidelines, the time step ($\Delta t = 0.005 \sim 0.01 L/U$) [ITTC, 2011] was taken at 0.04 seconds. The total resistance coefficient can be determined from the following formulae:

$$C_T = \frac{R_T}{0.5\rho U^2 S_{WS}}$$

Where,

R_T = Total Resistance;

ρ = Fluid Viscosity;

U = Speed;

S_{WS} = Wetted Surface Area;

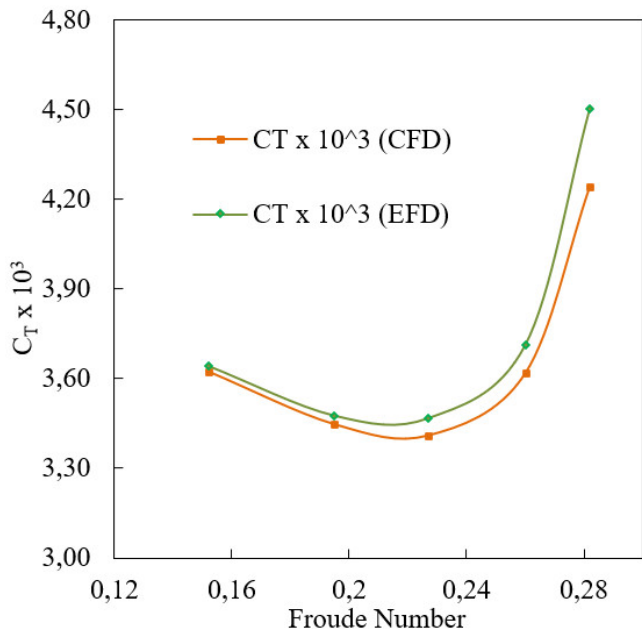
The total resistance of the parent hull for Froude number 0.26 from the simulation was 83.32N, and the total resistance coefficient was 3.6173×10^{-3} . From the simulation, the CFD value deviated around 2.525 %. Furthermore, the following data illustrates the comparison of CFD and EFD [Hino, et al., 2020] results for various Froude numbers.

Table 5: Comparison of the CFD Results with the Experimental Results at various Froude Number.

Froude Number	Total Drag (N)	$C_T \times 10^3$ (CFD)	$C_T \times 10^3$ [Exp. by Hino et al., 2020]	Deviation (%)
0.152	28.52	3.6232	3.641	0.49
0.195	44.66	3.4474	3.475	0.80
0.227	59.86	3.4103	3.467	1.64
0.26	83.32	3.6173	3.711	2.52
0.282	114.72	4.2402	4.501	5.79

Source: Authors.

Figure 6: Comparison of the Total Resistance Coefficient between CFD and EFD results.



Source: Authors.

The Table 6 shows the comparison between the first six cases with the parent hull having speed 2.196 m/s at Froude number 0.26.

Table 6: Resistance coefficient for different cases.

Case No.	Total Drag (N)	$C_T \times 10^3$ (CFD Modified Hull)	$C_T \times 10^3$ (CFD Parent Hull)	Deviation (%)
1	83.48	3.624	3.6173	0.19
2	83.34	3.618		0.02
3	83.8	3.638		0.58
4	83.22	3.613		-0.12
5	83.78	3.637		0.55
6	83.264	3.615		-0.07

Source: Authors.

The Table 7 compares Case 7’s simulated value to the parent hull with respect to improve hull at various Froude numbers.

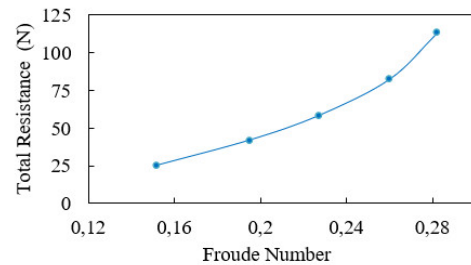
Table 7: Resistance coefficient for case 7 at various Froude numbers.

Froude Number	Total Drag (Improve hull) (N)	$C_T \times 10^3$ (CFD Improve hull)	$C_T \times 10^3$ (CFD Parent hull)	Decrease (%)
0.152	25.14	3.1938	3.6232	-11.85
0.195	41.92	3.2359	3.4474	-6.14
0.227	58.22	3.3169	3.4103	-2.74
0.26	82.44	3.5791	3.6173	-1.06
0.282	113.18	4.1833	4.2402	-1.34

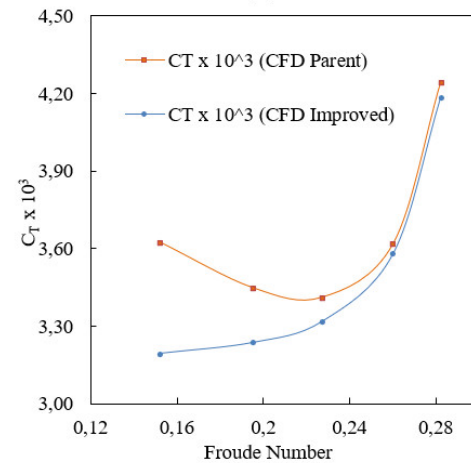
Source: Authors.

From Table 6, it can be seen that the resistance was reduced for only Case 4 and Case 6. Though the resistance is reduced, it is very minimal. For satisfactory results, Case 7 was simulated. From Table 7, the total resistance was 82.44 N and the total resistance coefficient was 3.579×10^{-3} , where it is 1.1 % less than the parent simulated hull and less than 3.56 % from the experimental value [Hino, et al., 2020] for Case 7.

Figure 7: (a) Total Resistance of hull with improved bow vs Froude number. (b) Comparison of Total Resistance Coefficient the Parent Hull with Hull of Improved Bow.



(a)



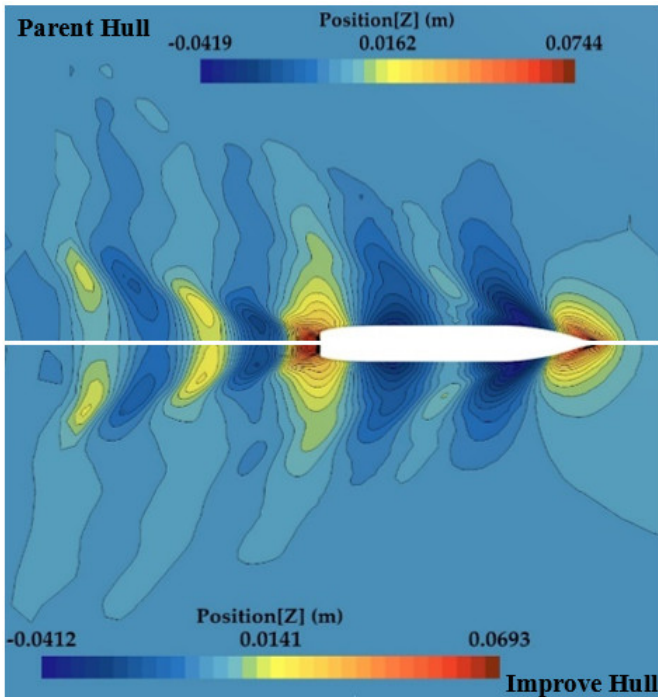
(b)

Source: Authors.

Figure 7 displays the relationship between the total resistance of the improve hull and the Froude number, as well as the resistance coefficients of the improve hull and the Froude number.

Comparison of the wave patterns produced by the parent and improve hull at Froude number 0.26 are illustrated below.

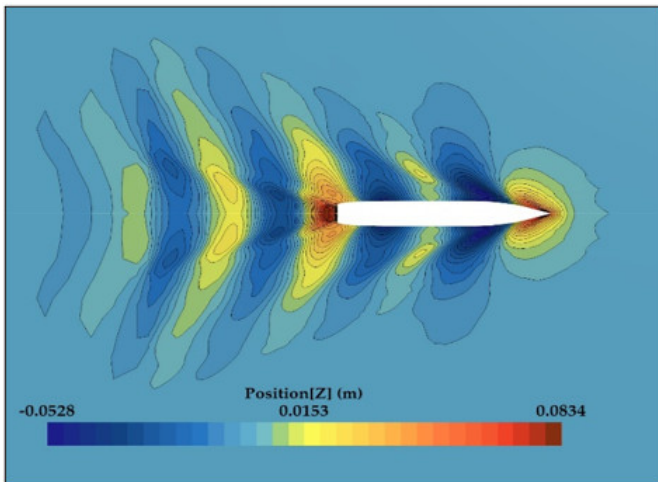
Figure 8: Comparison of the wave patterns at Froude Number 0.26.



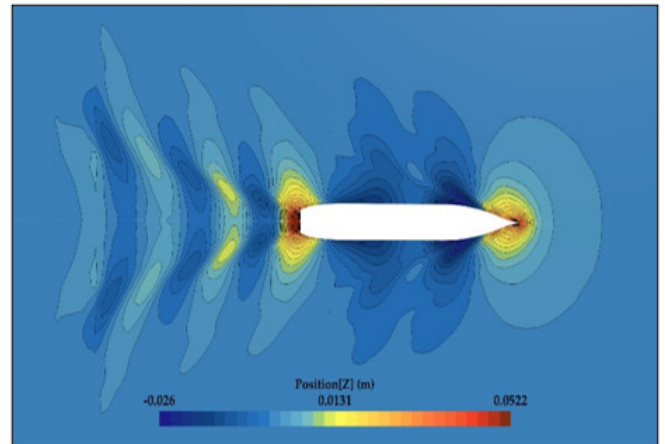
Source: Authors.

The wave patterns of improve hull for various Froude numbers of this case are illustrated below.

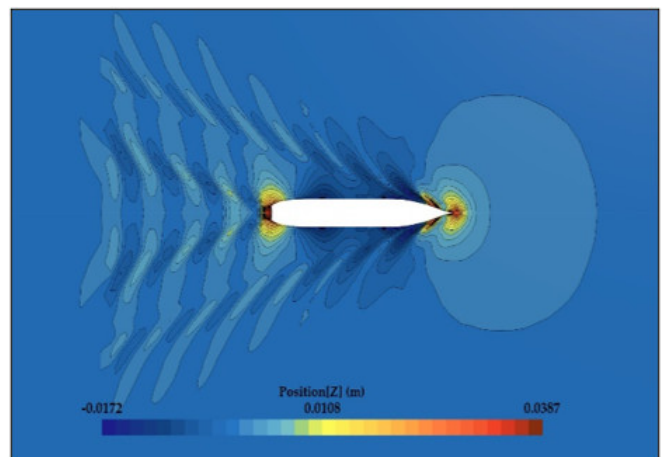
Figure 9: Wave Patterns of the improve hull at various Froude numbers (a-d).



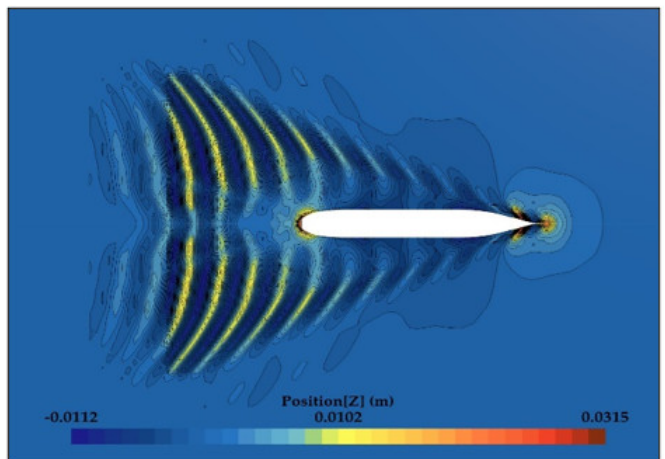
(a) Froude Number 0.282



(b) Froude Number 0.227



(c) Froude Number 0.195

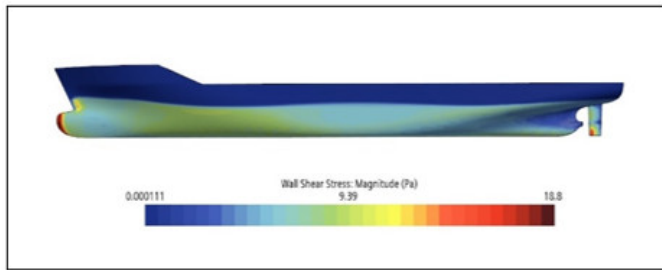


(c) Froude Number 0.152

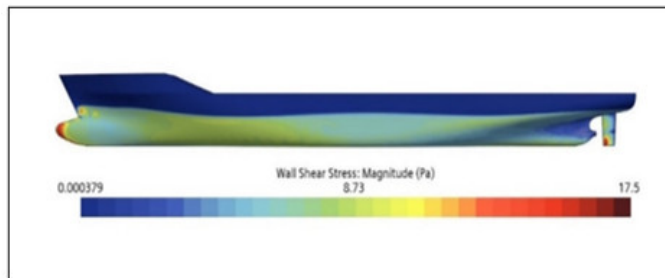
Source: Authors.

Comparison of wall shear stress between the parent hull and improve hull at Froude number 0.26 are illustrated in the Figure 10, in the next page.

Figure 10: Wall shear stress at Froude number 0.26. (a) Parent Hull. (b) Improve Hull.



(a)

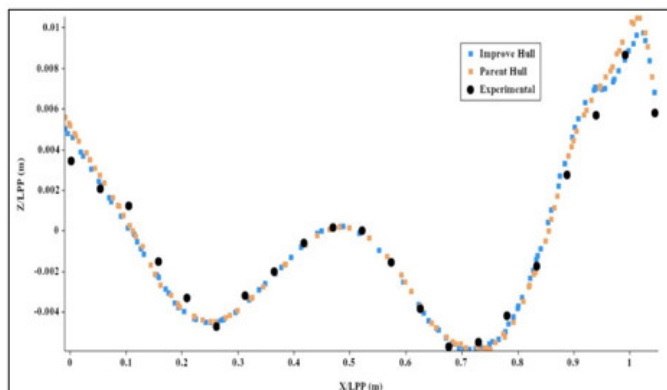


(b)

Source: Authors.

The following figure depicts the wave height on the outer surface of the KCS hull at a Froude Number of 0.26 for three separate circumstances.: experimental results [Hino, et al., 2020], the parent hull, the hull with improved bow.

Figure 11: Wave elevation on the hull surface.



Source: Authors.

The total resistance coefficient of the improve hull was significantly reduced for lower Froude numbers compared to the parent hull's value obtained using computational fluid dynamics (CFD). For a Froude number of 0.152, the total resistance coefficient fell by approximately 11.85%. All the wave Patterns of the improve hull at various Froude numbers effectively captured the Kelvin wake pattern. In Figure 6 and 7, the highest wave height is at the bow for both the parent and improve hulls

at all. It is 0.0744 meters for the parent hull and 0.0693 meters for the improve hull at Froude number 0.26. The lowest wave height is at the trough region for both hulls, where it is -0.0419 meters for the parent hull and -0.0412 meters for the improve hull at Froude number 0.26. Figure 8 illustrates the wall shear stress of the improve hull is also lesser compared to the parent hull. At the bow and rudder part, the maximum wall shear stress for the parent bow is 18.8 Pa, whereas for the improve hull it is 17.5 Pa. A comparison among the wave elevation generated for parent hull, improve hull, and the wave elevation measured experimentally. Figure 9 shows Z/L_{pp} versus X/L_{pp} from the middle of the ship. According to this, the improve hull has a lower wave elevation than the parent hull.

Conclusions.

A numerical study of the KRISO Container Ship (KCS) in calm water was conducted in STAR-CCM+ and the hull form was improved by the Free Form Deformation (FFD) method in CAESSES. The RANS method with $k - \epsilon$ turbulence model was selected for better accuracy and the VOF approach was used to capture the free surface. The bulbous bow shape was modified by altering various geometric parameters and all the bow shapes were simulated. Among them, Case 7 showed the best outcome where it reduced the total resistance coefficient from the CFD value of the parent hull by 11.85% at Froude number 0.152. As a result, the reduction in the total resistance coefficient of the improve hull is greater compared to the parent hull when the Froude number is lower. At lower Froude numbers, there is a more significant enhancement in performance due to less turbulence and more accuracy as compared to experimental results. The wave elevation as well as the wall shear stress is lower in the improve hull compared to the parent hull. The wave resistance will also be reduced. This will result in less fuel consumption and will give economic and environmental benefits. As a bulbous bow has a major effect on the performance of ships and the cost of operation, more concentration has to be given on identifying the bulbous bow's optimum geometric specifications by various optimization techniques for further decreasing the total resistance coefficient.

Acknowledgements.

The authors are thankful to Bangladesh University of Engineering and Technology for all of the assistances and supports.

References.

- Feng, Y.; Moctar, O. E.; Schellin, T. E. Parametric Hull Form Optimization of Containerships for Minimum Resistance in Calm Water and in Waves. *Journal of Marine Science and Application* **2021**, *20* (4), 670–693. <https://doi.org/10.1007/s11804-021-00243-w>.
- Franck, G., Mangini, S., Prende, H., Huespe, J., & Esquivel, Y. P. **2017**. Numerical simulation of large commercial ship navigation on Paraná river, Argentina. *VII International Conference on Computational Methods in Marine Engineering*.

Hao, H. Hull Form Optimization to Lower Resistance in Still Water and Added Resistance in Waves. *tore.tuhh.de* **2019**. <https://doi.org/10.15480/882.3351>.

Hino, T.; Stern, F.; Larsson, L.; Visonneau, M.; Hirata, N.; Kim, J. Numerical Ship Hydrodynamics - An Assessment of the Tokyo 2015 Workshop. *Springer* **2020**. <https://link.springer.com/book/10.1007/978-3-030-47572-7>.

Islam, H.; Ventura, M.; Soares, C.; Tadros, M.; Abdelwahab, H. S. Comparison between Empirical and CFD Based Methods for Ship Resistance and Power Prediction. In *CRC Press eBooks*; 2022; pp 347–357. <https://doi.org/10.1201/9781-003320272-38>.

ITTC – Recommended Procedures and Guidelines 7.5 – 03 – 02 – 03, **2011**, pp 11. <https://ittc.info/media/1357/75-03-02-03.pdf>.

Li, C.; Wang, Y.; Chen, J. Study on the Shape Parameters of Bulbous Bow of Tuna Longline Fishing Vessel. *International Conference on Energy and Environmental Protection (ICEEP)* **2016**. <https://doi.org/10.2991/iceep-16.2016.43>.

Liu, X.; Zhao, W.; Wan, D. Hull Form Optimization Based on Calm-Water Wave Drag with or without Generating Bulbous Bow. *Applied Ocean Research* **2021**, *116*, 102861. <https://doi.org/10.1016/j.apor.2021.102861>.

Nazemian, A.; Ghadimi, P. Automated CFD-Based Optimization of Inverted Bow Shape of a Trimaran Ship: Proposing an Applicable and Efficient Optimization Platform. *Scientia Iranica* **2020**. <https://doi.org/10.24200/sci.2020.56644.4833>.

Sederberg, T. W.; Parry, S. R. Free-Form Deformation of Solid Geometric Models. *Comput. Graph.* **1986**, *20* (4), 151–160. <https://doi.org/10.1145/15886.15903>.